CrossMark

ARTICLE

# Microstructure evolution in $L1_2$ hardened Co-base superalloys during creep

Yuzhi Li
*School of Materials Science and Engineering, Northwestern Polytechnical University, Xi'an 710072, China*

Florian Pyczak,[a] Jonathan Paul, Michael Oehring, and Uwe Lorenz
*Institute of Materials Research, Helmholtz-Zentrum Geesthacht, Geesthacht 21502, Germany*

Zekun Yao
*School of Materials Science and Engineering, Northwestern Polytechnical University, Xi'an 710072, China*

(Received 28 April 2017; accepted 21 August 2017)

The plastic deformation mechanisms and the microstructure development during creep deformation of $L1_2$-hardened Co-base superalloys show a number of unique features. The preferred orientation of rafting is determined by their positive lattice mismatch. In addition, the regular interfacial dislocation networks often found in rafted specimens of other types of superalloys do not form. While the ordered $\gamma'$-$L1_2$ precipitates are supposed to harden the material, they are actually found to be frequently cut by partial dislocations generating stacking faults. In this work, specimens from creep tests interrupted at different strains were investigated using transmission and scanning electron microscopy. By this, it is possible to find out which of these processes take place in which stage of creep deformation. For a better understanding of creep deformation, the balance between $\gamma'$ cutting and dislocation activity within the matrix channels is of special interest.

## I. INTRODUCTION

In 2006, a novel class of superalloys was discovered by Sato et al.[1] by their finding of a $\gamma'$-$Co_3(Al,W)$ phase with an $L1_2$ lattice structure in the ternary Co–Al–W system. For compositions exhibiting a $\gamma$-Co + $\gamma'$-$Co_3(Al,W)$ microstructure, the $\gamma'$-precipitates exhibit a cubic shape and are coherently embedded in a fcc $\gamma$-Co matrix. The precipitate sizes were in the range of some hundred nanometers with matrix channels of some ten nanometers in between and a $\gamma'$ volume fraction of up to 70%.[2,3] Depending on the W content of the alloy, the solvus temperature of the $\gamma'$ phase can be higher than 1000 °C. Other alloying elements, as, for example, Ta and Ti, were also found to increase the $\gamma'$ solvus temperature.[2] Taking all these observations into account and keeping in mind that Ni-base superalloys, which exhibit similar microstructures and properties, are very successful high-temperature materials, the Co–Al–W system has a good potential to be an attractive material for high-temperature applications.[4–8]

Despite the high similarity of the $\gamma/\gamma'$ microstructures between these novel Co-base and the well-known Ni-base superalloys, the creep and high-temperature plastic deformation mechanisms seem to differ between the two alloy classes. In the high-temperature regime at around 850–1000 °C, creep deformation in Ni-base superalloys is dominated by the dislocation movement in the $\gamma$ matrix channels.[9,10] Depending on the lattice mismatch between the $\gamma$ matrix and $\gamma'$ phase and the externally applied stress, one orientation of matrix channels with respect to the externally applied stress deforms first, while plastic deformation in the other orientation of matrix channels is delayed. Dislocations moved up to the $\gamma/\gamma'$ interfaces rearrange there to build interfacial dislocation networks, which can partly compensate for coherency stresses between the $\gamma$ matrix and $\gamma'$ precipitate phase.[9,10] Given a sufficiently high creep temperature, a process known as rafting also takes place, where the $\gamma'$ precipitates coarsen together.[9,11] This process generates a microstructure of $\gamma'$ plates perpendicular or $\gamma'$ rods parallel to the external stress axis, depending on the sign of the external stress and the $\gamma/\gamma'$ lattice mismatch.[9,10] With dislocations filling the matrix channels and the development of the raft structure, dislocation movement within the matrix channels and the transfer of dislocations from one orientation of matrix channels to the other become increasingly difficult.[12] Then also plastic deformation of the stronger ordered intermetallic $\gamma'$ phase is necessary. This happens by cutting through the $\gamma'$ rafts by pairs of ordinary dislocations with an antiphase boundary between them.[12,13]

$\gamma'$ hardened Co-base superalloys show some striking dissimilarities to the behavior of Ni-base superalloys.

Contributing Editor: Mathias Göken
[a]Address all correspondence to this author.
e-mail: florian.pyczak@hzg.de
DOI: 10.1557/jmr.2017.362

https://doi.org/10.1557/jmr.2017.362 Published online by Cambridge University Press

 © Materials Research Society 2017

These differences are especially pronounced for ternary Co–Al–W alloys. It seems that dislocation activity is confined to only one orientation of matrix channels until plastic strains of up to at least 3–4%.[14] These dislocations also do not form nicely ordered dislocation networks as seen in Ni-base superalloys. But, the most striking difference when compared to Ni-base superalloys is the large number of stacking faults in the $\gamma'$ particles,[5,14] which suggests that $\gamma'$ particles are frequently cut by super partials during creep deformation. Titus et al.[15] found superlattice intrinsic and extrinsic stacking faults in crept ternary and Ta-containing Co-base alloys. These facilitated $\gamma'$ cutting, and both W and Ta were found to segregate at these stacking faults.[16] The arrangement of these stacking faults locally changed the crystal structure to the $D0_{19}$-$Co_3W$ phase. Recently, Eggeler et al.[17] analyzed in high detail the structure of planar defects present in $\gamma'$ precipitates of a CoNi alloy and found them to be a complex arrangement of super partial and partial dislocations separated by the corresponding stacking faults and antiphase boundaries. Conclusively, it can be stated that the $\gamma'$ precipitate cutting by partial and super partial dislocations leaving respective planar faults within the $\gamma'$ particles is a common deformation mechanism during the creep of $\gamma'$-hardened Co-base superalloys. Unfortunately, not much data about the development of the microstructure and deformation structures during creep of $\gamma'$-hardened Co-base superalloys is available yet.[14,18] To better understand and improve these alloys, it is of utmost importance to know if $\gamma'$ cutting or deformation of matrix channels by dislocations is the mechanism that takes place first during creep deformation. In addition, the onset of these different plastic deformation mechanisms with respect to the different stages of creep and the degree of rafting present in the material are of interest.

In the present work, creep tests performed on ternary Co–Al–W alloys were interrupted at different strains, and the crept material was investigated using scanning electron microscopy (SEM) and transmission electron microscopy (TEM).

## II. EXPERIMENTAL

Three alloys with the nominal composition Co–9Al–$x$W ($x$ = 8, 9, and 11; all in atomic percent) were initially prepared from their elements and cast as rods in an arc melting furnace. Subsequently, the material was used to cast single crystalline rods of 5 mm diameter using a pigtail grain selector in a Bridgman casting device at the University of Bayreuth. For sake of brevity, from now on these alloys will be termed 8W, 9W, and 11W. The material was solution heat-treated at 1300 °C for 12 h in a vacuum furnace. Subsequently, the material was aged at 900 °C for 200 h in air. From this standard heat-treated material, cylindrical creep compression specimens of 7.5 mm height and 5 mm diameter were prepared by electrodischarge machining and grinding. To ensure that the specimens are oriented parallel to the ⟨001⟩ direction, they were aligned using electron backscattered diffraction in the SEM prior to fabrication. Due to problems during the casting, only few specimens with suited ⟨001⟩ orientation could be prepared of 11W. Thus, the complete investigation program conducted on 8W and 9W could not be performed with 11W. 11W results are nevertheless included for comparison.

The compression creep tests were conducted in air using a Satec Systems creep machine (Instron, Norwood, Massachusetts) with a lever arm ratio of 16:1 at a temperature of 850 °C and a constant applied load corresponding to an initial stress of either 400 or 460 MPa.

For microstructure characterization sections of the crept specimens perpendicular to the stress axis and of the {100}/{010} plane parallel to the stress axis were cut. For SEM characterization, they were ground, mechanically polished, and finally electro polished for 90 s with a solution of 2-buthanol and perchloric acid in methanol at −41 °C using a voltage of 25 V. TEM specimens were prepared by cutting thin slices in the orientations mentioned above. These were mechanically ground down to a thickness of about 60 μm. Subsequently, these foils were electrolytically thinned to electron transparency with a Struers A3 electrolyte (Struers GmbH, Willich, Germany) and a voltage of 20 V at −38 °C.

For SEM investigations, a LEO Gemini 1530 SEM with a field emission gun (Carl Zeiss AG. Oberkochen, Germany) was used in the backscattered electron mode. TEM characterization was performed with a FEI (Hillsboro, Oregon) CM200 operated at 200 kV.

## III. RESULTS AND DISCUSSION

All three alloys exhibited a $\gamma/\gamma'$ microstructure with cubic $\gamma'$ precipitates in the state prior to creep testing. With increasing the W content, the fraction of the $\gamma'$ phase increased, the $\gamma'$ precipitates were bigger, and the matrix channels were narrower. Nevertheless, the differences in microstructure between 8W and 9W, which are the two alloys most thoroughly investigated in this work, were less pronounced than those between these two and 11W. In Fig. 1, the microstructures of the three alloys are imaged using TEM. The alloys 8W and 9W exhibit mostly cubic $\gamma'$ precipitates of about 100–200 nm in size that are aligned along ⟨100⟩ directions. The cube corners are rounded, and a number of precipitates deviating in size and shape from the average of about 200 nm cubes are interdispersed. The precipitates in 11W are larger with sharper corners [Fig. 1(c)]. In the broad matrix regions between the $\gamma'$ precipitates of 8W, a large number of secondary $\gamma'$ precipitates are visible, which were absent in 9W and 11W.

https://doi.org/10.1557/jmr.2017.362 Published online by Cambridge University Press

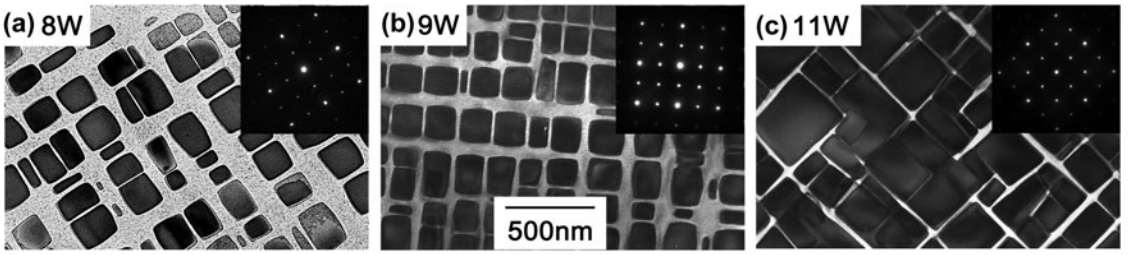



FIG. 1. Microstructure of (a) 8W, (b) 9W, and (c) 11W after solution heat treatment and aging for 200 h at 900 °C, representing the microstructure prior to creep testing; the image was taken using TEM in the multibeam condition. The inset shows the corresponding diffraction pattern.

Figure 2 shows strain rate against strain ($\dot{\varepsilon}$–$\varepsilon$) curves for creep tests performed at 850 °C on the 8W, 9W, and 11W alloys. As 8W exhibited worse creep resistance than 9W, in one test it was loaded to a stress of 400 MPa so that the time to 3–4% plastic strain was close to that for 9W loaded at 460 MPa. The creep tests were terminated at 3.9% plastic strain after 70 h for 8W under a load of 400 MPa and at 2.9% after 53 h for 9W under a load of 460 MPa. Both alloys show a primary creep stage with rapid hardening until they both reach a minimum creep rate of about $6 \times 10^{-8}$ $s^{-1}$. After that point, the specimens are softening. In 8W, this softening decelerates on further deformation to reach a nearly constant creep rate between about 1 and 4% plastic strain. On the contrary, the 9W specimen shows continuous softening after the creep minimum. When 8W was tested under a load of 460 MPa, it shows a less pronounced and a higher creep minimum of about $3 \times 10^{-7}$ $s^{-1}$, while the alloy 11W has a much higher creep resistance exhibiting a minimum creep rate of about $2 \times 10^{-8}$ $s^{-1}$ and a longer primary creep stage. The reason for the latter is unknown. The following more detailed characterization of the microstructure was restricted to interrupted tests of 8W under a load of 400 MPa and 9W under a load of 460 MPa.

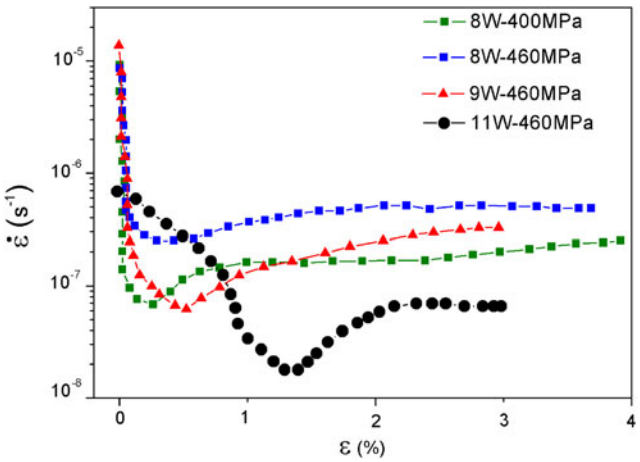



FIG. 2. Strain rate versus strain curves of 8W, 9W, and 11W tested at 850 °C.

Figure 3 shows SEM micrographs of specimens of 8W which were crept to different plastic strains. While the specimens after 0.07 and 0.45% of strain, the latter being about the creep rate minimum, show cubic shape and are aligned along different ⟨001⟩ directions in the specimens deformed to higher creep strains, a clear alignment perpendicular to the external stress axis is visible. In addition, some of the γ′ particles now appear elongated perpendicular to the stress axis probably because the former γ′ cubes have fused together. This process is well known from Ni-base superalloys as directional coarsening or rafting.[9,10,19,20]

The development of the γ/γ′ microstructure in the 9W alloy with increasing creep strain is shown in Fig. 4. The images correspond to creep specimens that were interrupted after 0.07, 0.4, 1.1, and 3% plastic strain. The specimen interrupted at 0.4% strain represents the microstructure near the minimum creep rate. As in the case of the 8W alloy, no preferential alignment along one of the ⟨100⟩ directions or rafting of γ′ precipitates is discernible before the minimum creep rate was attained in the 9W alloy at 0.4% creep strain. In the two specimens from tests that were terminated at strains of 1.1 and 3%, the γ′ precipitates align perpendicular to the external stress axis and coarsen together forming a rafted γ/γ′ microstructure.

Thus the preferential direction for rafting was perpendicular to the external compressive stress axis for both alloys. In Ni-base superalloys, this is the expected direction for rafting under a compressive load for an alloy exhibiting a positive lattice mismatch between the γ and γ′ phases at the creep temperature.[9] It is known for a Co-base ternary alloy with a similar composition to 9W that it had a positive lattice mismatch at 850 °C.[21] Thus, it is assumed that also for 8W and 9W in the present study, the lattice mismatch was positive at the creep temperature. Qualitatively, it seemed that rafting of the γ′ particles took place after the creep minimum. To get quantitative data about the morphological development of the γ′ precipitates by line intersection method, the length of γ′ precipitates using the lines perpendicular to the external stress axis and the width of the matrix channels perpendicular to the external stress axis (i.e., horizontal)

https://doi.org/10.1557/jmr.2017.362 Published online by Cambridge University Press

using lines parallel to the external stress axis were measured. In each alloy, at least 200 particles from four separate micrographs were considered. The respective results are shown in Fig. 5.

It is clearly visible that in both alloys the length of γ′ precipitates abruptly increases for strains larger than 1% [Fig. 5(a)]. This is in good agreement with the qualitative observation from the SEM micrographs. The abrupt increase of the γ′ length also hints to the fact that the rafting does take place by a meet and fusing together with adjacent γ′ particles as described by Nabarro[9] for later stages of rafting. By such a process, the length of the precipitates increases strongly at the point where a fusing together[9] or coalescence[11] takes place and afterward stays more or less on the same level. On the contrary as shown in Fig. 5(b), a linear increase of the width of the γ matrix channels perpendicular to the external stress axis (i.e., the matrix channels being horizontal in Figs. 3 and 4) when plotted over ln(ε) is found, as expected for a diffusion-controlled coarsening.

The development of the deformation structures in both alloys was characterized by TEM. Figure 6 shows micrographs of the crept 8W alloy after varying degrees of creep deformation. TEM images were taken from foils oriented parallel [Figs. 6(a)–6(d)] and perpendicular [Figs. 6(e)–6(h)] to the external stress axis. It is noteworthy that cutting of γ′ precipitates associated with stacking faults already takes place at a very low strain of 0.07%, [Fig. 6(a)] which is well within the primary creep regime. When compared to Ni-base superalloys, this is surprising as the onset of plastic deformation in the softer unordered matrix phase is expected to take place earlier, while the stronger ordered intermetallic γ′ precipitates tend to deform later.[12] This may indicate that at least in

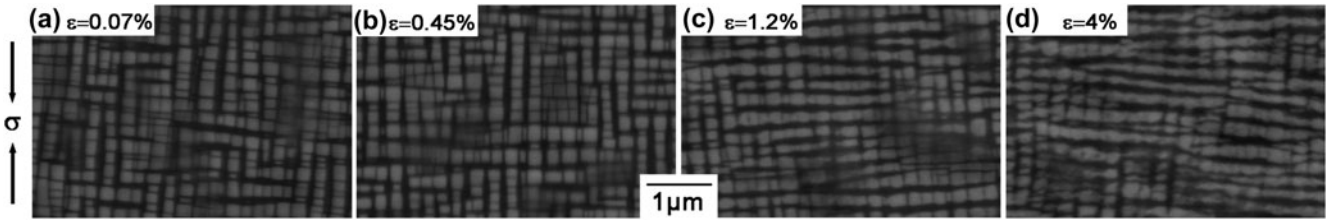



FIG. 3. Microstructure development of γ′ precipitates in 8W after creep at 850° under 400 MPa to (a) 0.07%, (b) 0.45%, (c) 1.2%, and (d) 4% plastic strain.

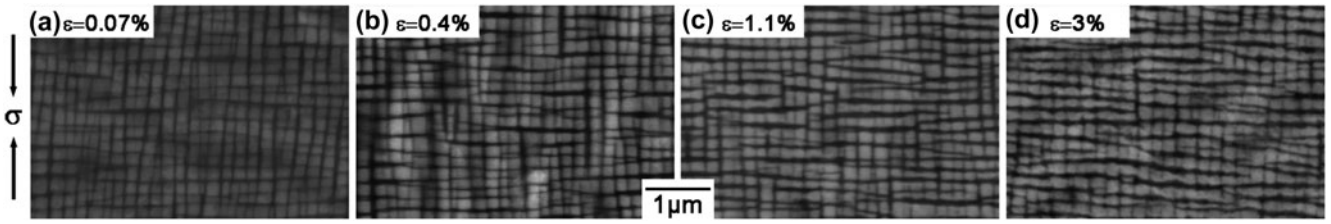



FIG. 4. Microstructure development of γ′ precipitates in 9W after creep at 850° under 460 MPa to (a) 0.07%, (b) 0.4%, (c) 1.1%, and (d) 3% plastic strain.

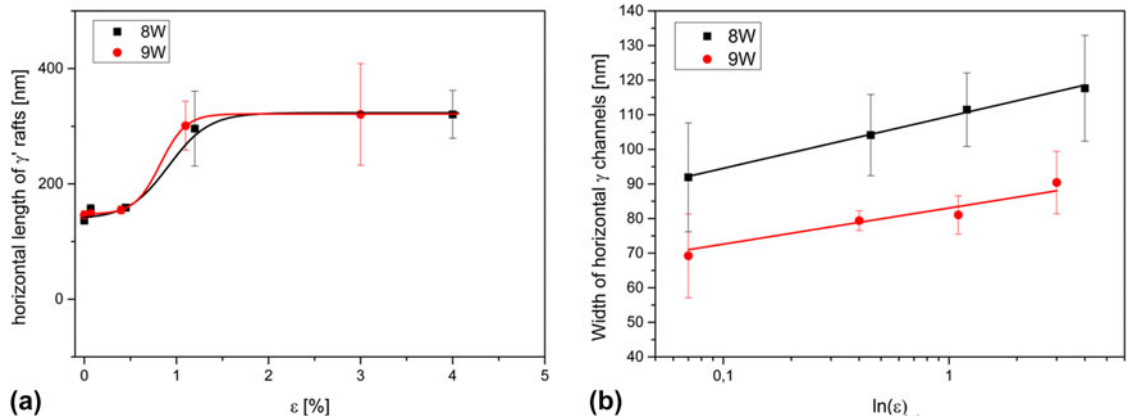



FIG. 5. (a) Length of γ′ precipitates in crept specimens of the 8W and 9W alloys measured along the direction perpendicular to the external stress axis; (b) width of horizontal γ matrix channels in crept specimens of alloys 8W and 9W measured in the direction parallel to the stress.



https://doi.org/10.1557/jmr.2017.362 Published online by Cambridge University Press

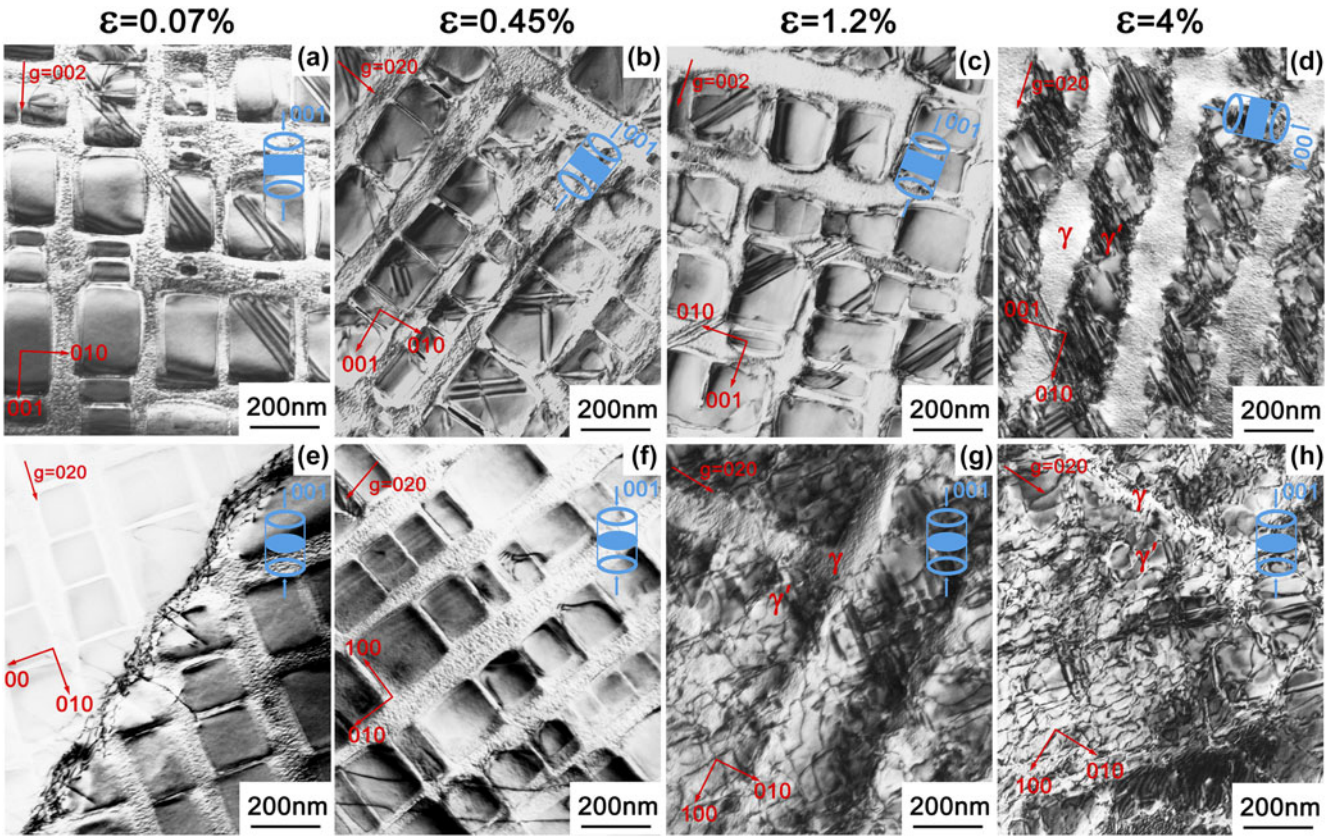



FIG. 6. Deformation structures of the 8W alloy—upper row: TEM foil parallel to stress axis (a) 0.07%, (b) 0.45%, (c) 1.2%, and (d) 4% plastic strain—lower row: TEM foil perpendicular to the stress axis (e) 0.07%, (f) 0.45%, (g) 1.2%, and (h) 4% plastic strain, deformed under a load of 400 MPa at 850 °C.

these ternary Co–Al–W alloys, the $Co_3(W,Al)$ $L1_2$ phase is much softer and more deformable relative to the Co-matrix than the corresponding $Ni_3Al$ $L1_2$ phase relative to the Ni-matrix in Ni-base superalloys. The occurrence of stacking faults will also be discussed later in relation to the W content of the alloys. Except for a subgrain boundary pictured in Fig. 6(e), which could also have been already present in the material prior to the creep test, the first signs of dislocation activity are found at 0.4% strain. At this strain, single nearly straight dislocation segments spanning over a number of matrix channels and $\gamma'$ precipitates are clearly seen in the $\gamma$ matrix channels perpendicular to the stress axis [Fig. 6(f)]. As the creep strain increases to 1.2 and 4%, the dislocation activity in the matrix channels perpendicular to the stress axis [Figs. 6(g) and 6(h)] strongly increases. These dislocations are not straight and regular anymore but appear to have a kind of entangled irregular arrangement. Meanwhile the matrix channels parallel to the stress axis [Figs. 6(c) and 6(d)] are virtually free of dislocations.

Figure 7 shows a series of TEM micrographs taken from interrupted creep specimens of the 9W alloy crept to 0.07, 0.4, 1.1, and 3% creep strains. The phenomena observed are generally similar to those seen in the 8W alloy. Again cutting of $\gamma'$ precipitates has already taken place during the initial stages of creep, as indicated by the presence of stacking faults [Fig. 7(a)]. Such $\gamma'$ precipitate cutting during the primary creep was already reported by Shi et al.[18] for a more complex Co–Al–W–Ni–Ti alloy. Recently Zhou et al. also reported the occurrence of planar faults already during early creep deformation in a Co–Al–W–Ta–Ti alloy.[22] It is observable, especially in the specimens deformed up to higher creep strains that the dislocation activity in matrix channels perpendicular to the stress axis [Figs. 7(g) and 7(h)] is much stronger than in matrix channels parallel to the stress axis [Figs. 7(c) and 7(d)]. The latter appear to be nearly free of dislocations, which is similar to the observations in the 8W alloy. Nevertheless, in some details, the deformation structures in specimens of 9W and 8W alloys differ. The onset of dislocation activity takes place earlier in 9W, and some straight dislocation segments spanning over a number of $\gamma'$ precipitates and matrix channels are already visible in the primary stage of creep at 0.07% strain [Fig. 7(e)]. A strong dislocation activity in the matrix channels perpendicular to the stress axis is found in specimens deformed up to the creep minimum and above, i.e., to 0.4, 1.1,

https://doi.org/10.1557/jmr.2017.362 Published online by Cambridge University Press

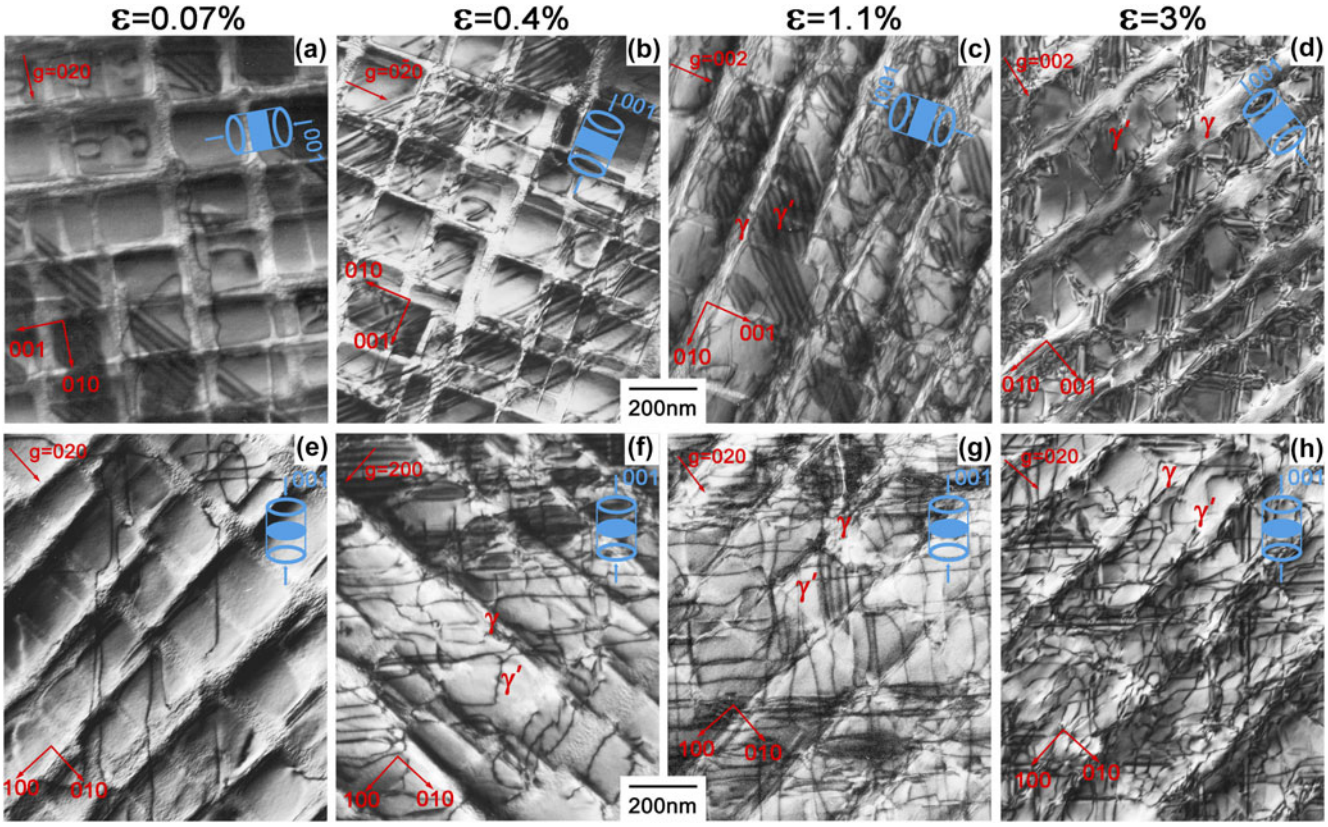



FIG. 7. Deformation structures in alloy 9W—upper row: TEM foil parallel to stress axis (a) 0.07%, (b) 0.4%, (c) 1.1%, and (d) 3% plastic strain—lower row: TEM foil perpendicular to stress axis (e) 0.07%, (f) 0.4%, (g) 1.1%, and (h) 3% plastic strain, deformed with a load of 460 MPa at 850 °C.

and 3% of strain, respectively, as is visible in Figs. 7(f)–7(h). Despite this strong dislocation activity, no well-developed dislocation networks as known from Ni-base alloys deformed under similar creep conditions have been found. However, some of the dislocation segments seemed to have interacted with each other forming rounded corners similar to dislocation arrangements already reported in a ternary Co–9Al–9W alloy earlier by Pyczak et al.[14] and also observed during the first stages of dislocation network formation in Ni-base superalloys by Field et al.[23] In general, the dislocation structure in 9W appears more regular than in 8W.

The earlier onset of dislocation activity in one orientation of matrix channels can be explained by the combined effect of external applied stress and the coherency stresses, which are due to the $\gamma/\gamma'$ lattice mismatch. While in one orientation of matrix channels the coherency stress and the externally applied stress add up, they counteract each other in the other orientation of matrix channels. Dislocation activity starts in the orientation of matrix channels, where the coherency stress increases the externally applied stress causing a higher local stress and thus earlier plastic deformation. In the case of Co-base alloys deformed in compression, these should be the matrix channels perpendicular to the external stress axis, assuming, as is here the case, that the $\gamma/\gamma'$ lattice mismatch is positive at the creep temperature. While measurements of lattice mismatch at elevated temperatures are still scarce for Co-base superalloys, data available in the literature report positive values for Co-rich systems.[7,14,21,24,25] Nevertheless, no well-developed dislocation networks are observed. This could be explained by the role of the $\gamma/\gamma'$ lattice mismatch and the coherency stresses induced by it. When dislocation activity takes place in matrix channels, where the coherency stresses add up with the externally applied stress, the dislocations cause a plastic deformation that relaxes the coherency stresses. Thus, it is energetically favorable to store these dislocations at the $\gamma/\gamma'$ interfaces in a configuration of regular dislocation networks.[23,26] The higher the amount of $\gamma/\gamma'$ lattice mismatch the higher the driving force to build such regular dislocation networks. As already mentioned Co-base superalloys exhibit a positive lattice mismatch at room temperature, which decreases to smaller positive values with increasing temperature. Thus, the amount of lattice mismatch and the driving force to form dislocation networks is low. On the contrary, many Ni-base superalloys have a negative lattice mismatch at room temperature that becomes more negative with increasing the temperature (e.g., Ref. 27). Thus, the

https://doi.org/10.1557/jmr.2017.362 Published online by Cambridge University Press

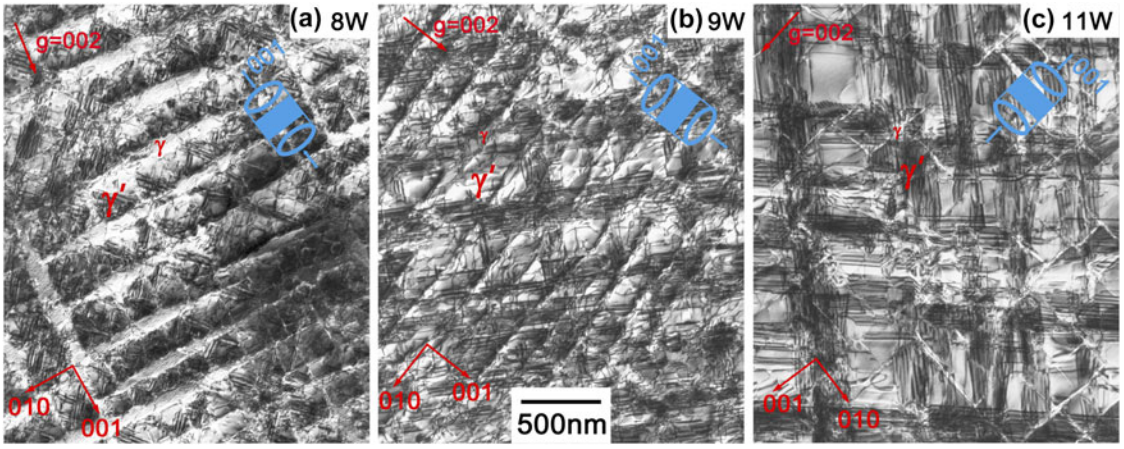



FIG. 8. Deformation structures imaged in TEM foils orientated perpendicular to the stress axis in (a) the 8W alloy at 3.6% strain (460 MPa @ 850 °C), (b) the 9W alloy at 3% strain (460 MPa @ 850 °C), and in (c) the 11W alloy at 3.6% strain (460 MPa @ 850 °C).

amount of lattice mismatch and the driving force to build regular dislocation networks increases with temperature in most Ni-base superalloys. This is a possible explanation why no regular dislocation networks are found in Co-base superalloys as compared to Ni-based superalloys. The amount of $\gamma/\gamma'$ lattice mismatch and, thus, the driving force to build regular dislocation networks are lower in the Co-based alloys. It should be noted that the easiness of $\gamma'$ cutting observed in these Co-based alloys[28,29] and discussed above may also contribute to the absence of regular dislocation networks. Dislocations stopped at the $\gamma/\gamma'$ interfaces could dissociate into partial or super partial dislocations, which are able to cut the $\gamma'$ precipitates and hence fewer dislocations remain at the $\gamma/\gamma'$ interfaces to form networks.

In Ni-base superalloys, it is commonly accepted that rafting of the $\gamma'$ phase is due to the presence of interfacial dislocation networks at the $\gamma/\gamma'$ interfaces.[30,31] Nevertheless, it was predicted by Pineau[32] that purely elastic strains and stresses could also cause a rafting-like elongation of precipitates. For Co-base superalloys, it still has to be clarified whether the rafting observed during creep deformation is an effect of plastic deformation, i.e., the presence of dislocations at the $\gamma/\gamma'$ interfaces or caused by elastic distortions resulting from a lattice mismatch.

To investigate the role of the $\gamma'$ volume fraction on the deformation mechanisms during creep specimens from the 8W, the 9W, and 11W alloys that had been deformed to between 3 and 4% creep strain were compared using TEM. Micrographs from TEM foils that were perpendicular to the external stress axis (i.e., with viewing direction parallel to the external stress axis) are shown in Fig. 8. The most obvious difference between the alloys is an increase of stacking fault density, which increases in the order 8W, 9W, and 11W. There are two possible explanations for this. One possibility is that due to the different chemical compositions of the alloys, it may be easier to cut through the $\gamma'$ precipitates in higher W-containing alloys. Alternatively, to achieve a compatible deformation of both the $\gamma$ and $\gamma'$ phases, it is necessary that more frequent $\gamma'$ cutting occurs in the alloy with the higher $\gamma'$ volume fraction. Normally, the former explanation could be ruled out because according to the ternary Co–Al–W phase diagram published by Sato et al.,[1] the chemical composition of the $\gamma'$ phase should not change significantly when the W content is changed within the $\gamma/\gamma'$ two-phase field. Thus, the $\gamma'$ phase in all three alloys should have a more or less similar chemical composition and, therefore, the ease of cutting the $\gamma'$ precipitates should be similar in all three alloys. Nevertheless, it is an ongoing discussion whether the $\gamma'$ phase is thermodynamically stable in the Co–Al–W system.[21,33–35] If the $\gamma'$ phase is not stable, then the phase diagram of Sato et al. is not applicable. It is noteworthy in this case that Titus et al.[16] found that the cutting of $\gamma'$ particles could locally change the crystal structure to a $D0_{19}$ type. Therefore, the cutting of $\gamma'$ particles could be connected with the transformation from the metastable $L1_2$ $Co_3(Al,W)$ $\gamma'$ phase to the thermodynamically stable $D0_{19}$ $Co_3W$ phase, which could accelerate the process of $\gamma'$ cutting by super partial dislocations. Since the phase stability is expected to depend on the W concentration, differences in the stacking fault density and phase transformation kinetics between the alloys can easily be understood.

## IV. CONCLUSIONS

Ternary Co–Al–W alloys were creep deformed to analyze the plastic deformation mechanisms and development of the $\gamma/\gamma'$ microstructure during the different stages of creep. While some similarities to Ni-base superalloys with related microstructures were observed, the Co–Al–W alloys also showed features that are unique to this material class:

https://doi.org/10.1557/jmr.2017.362 Published online by Cambridge University Press

(1) Rafting of $\gamma'$ precipitates takes place after the minimum creep rate has been reached and the preferred orientation of the rafts is in accordance with the positive $\gamma/\gamma'$ lattice mismatch of the alloys at creep temperature.

(2) The cutting of $\gamma'$ precipitates by partial dislocations, which generates stacking faults in the $\gamma'$ particles is a process which already takes place during the early stages of creep deformation.

(3) Dislocation activity in the $\gamma$ matrix is strongly confined to one orientation of matrix channels, where plastic deformation is favored due to the combined $\gamma/\gamma'$ coherency stresses and the externally applied stress.

(4) No formation of regular dislocation networks at the $\gamma/\gamma'$ interfaces is observed.

(5) Cutting of $\gamma'$ precipitates occurs more frequently in alloys with a higher W content and a higher $\gamma'$ volume fraction.

## REFERENCES


1. J. Sato, T. Omori, K. Oikawa, I. Ohnuma, R. Kainuma, and K. Ishida: Cobalt-base high-temperature alloys. *Science* **312**, 90 (2006).
2. A. Bauer, S. Neumeier, F. Pyczak, and M. Göken: Microstructure and creep strength of different $\gamma/\gamma'$-strengthened Co-base superalloy variants. *Scr. Mater.* **63**, 1197 (2010).
3. T.M. Pollock, J. Dibbern, M. Tsunekane, J. Zhu, and A. Suzuki: New Co-based $\gamma$–$\gamma'$ high temperature alloys. *JOM* **62**, 58 (2010).
4. A. Suzuki, G.C. DeNolf, and T.M. Pollock: Flow stress anomalies in $\gamma/\gamma'$ two-phase Co–Al–W-base alloys. *Scr. Mater.* **56**, 385 (2007).
5. A. Suzuki and T.M. Pollock: High-temperature strength and deformation of $\gamma/\gamma'$ two-phase Co–Al–W-base alloys. *Acta Mater.* **56**, 1288 (2008).
6. A. Bauer, S. Neumeier, F. Pyczak, R.F. Singer, and M. Göken: Creep properties of different $\gamma'$-strengthened Co-base superalloys. *Mater. Sci. Eng., A* **550**, 333 (2012).
7. A. Bauer, S. Neumeier, F. Pyczak, and M. Göken: Creep strength and microstrcuture of polycrystalline $\gamma'$-strengthened cobalt-base superalloys. In *Superalloys 2012*, E.S. Huron, R.C. Reed, M.C. Hardy, M.J. Mills, R.E. Montero, P.D. Portella, and J. Telesman, eds. (The Minerals, Metals & Materials Society, Warrendale, PA, 2012); p. 695.
8. H. Mughrabi: The importance of sign and magnitude of $\gamma/\gamma'$ lattice misfit in superalloys—with special reference to the new $\gamma'$-hardened cobalt-base superalloys. *Acta Mater.* **81**, 21 (2014).
9. F.R.N. Nabarro: Rafting in superalloys. *Metall. Trans. A* **27**, 513 (1996).
10. H. Mughrabi and U. Tetzlaff: Microstructure and high-temperature strength of monocrystalline nickel-base superalloys. *Adv. Eng. Mater.* **2**, 319 (2000).
11. T.M. Pollock and A.S. Argon: Directional coarsening in nickel-base single crystals with high volume fractions of coherent precipitates. *Acta Metall. Mater.* **42**, 1859 (1994).
12. T.M. Pollock and A.S. Argon: Creep resistance of CMSX-3 nickel base superalloy single crystals. *Acta Metall. Mater.* **40**, 1 (1992).
13. T. Link and M. Feller-Kniepmeier: Shear mechanisms of the $\gamma'$ phase in single-crystal superalloys and their relation to creep. *Metall. Trans. A* **23**, 99 (1992).
14. F. Pyczak, A. Bauer, M. Göken, S. Neumeier, U. Lorenz, M. Oehring, N. Schell, A. Schreyer, A. Stark, and F. Symanzik: Plastic deformation mechanisms in a crept $L1_2$ hardened Co-base superalloy. *Mater. Sci. Eng., A* **571**, 13 (2013).
15. M.S. Titus, Y.M. Eggeler, A. Suzuki, and T.M. Pollock: Creep-induced planar defects in $L1_2$-containing Co- and CoNi-base single-crystal superalloys. *Acta Mater.* **82**, 530 (2015).
16. M.S. Titus, A. Mottura, G.B. Viswanathan, A. Suzuki, M.J. Mills, and T.M. Pollock: High resolution energy dispersive spectroscopy mapping of planar defects in $L1_2$-containing Co-base superalloys. *Acta Mater.* **89**, 423 (2015).
17. Y.M. Eggeler, J. Müller, M.S. Titus, A. Suzuki, T.M. Pollock, and E. Spiecker: Planar defect formation in the $\gamma'$ phase during high temperature creep in single crystal CoNi-base superalloys. *Acta Mater.* **113**, 335 (2016).
18. L. Shi, J.J. Yu, C.Y. Cui, and X.F. Sun: Microstructural stability and tensile properties of a Ti-containing single-crystal Co–Ni–Al–W-base alloy. *Mater. Sci. Eng., A* **646**, 45 (2015).
19. H. Mughrabi: $\gamma/\gamma'$ rafting and its effect on the creep and fatigue behaviour of monocrystalline superalloys. In *The Johannes Weertmann Symposium*, R.J. Arsenault, D. Cole, T. Gross, G. Kostorz, P.K. Liaw, S. Parameswaran, and H. Sizek, eds. (The Minerals, Metals & Materials Society, Warrendale, PA, 1996); p. 267.
20. J. Hammer and H. Mughrabi: High temperature creep and microstructure of the monocrystaline nickel-base superalloys SRR 99. In *EUROMAT 89*, H.E. Exner and V. Schuhmacher, eds. (Proceedings of the First European Conference on Advanced Materials and Processes, DGM Informationsgesellschaft Verlag, Oberursel 1990); p. 445.
21. F. Pyczak, A. Bauer, M. Göken, U. Lorenz, S. Neumeier, M. Oehring, J. Paul, N. Schell, A. Schreyer, A. Stark, and F. Symanzik: The effect of tungsten content on the properties of $L1_2$-hardened Co–Al–W alloys. *J. Alloys Compd.* **632**, 110 (2015).
22. H.J. Zhou, H. Chang, and Q. Feng: Transient minimum creep of a $\gamma'$ strengthened Co-base single-crystal superalloy at 900 °C. *Scr. Mater.* **135**, 84 (2017).
23. R.D. Field, T.M. Pollockf, and W.H. Murphy: The development of $\gamma/\gamma'$ interfacial dislocation networks during creep in Ni-base superalloys. In *Superalloys 1992*, S.D. Antolovich, R.W. Stusrud, R.A. MacKay, D.L. Anton, T. Khan, R.D. Kissinger, and D.L. Klarstrom, eds. (The Minerals, Metals & Materials Society, Warrendale, PA, 1992); p. 557.
24. K. Tanaka, M. Ooshima, N. Tsuno, A. Sato, and H. Inui: Creep deformation of single crystals of new Co–Al–W-based alloys with fcc/$L1_2$ two-phase microstructures. *Philos. Mag.* **92**, 4011 (2012).
25. H-Y. Yan, V.A. Vorontsov, J. Coakley, N.G. Jones, H.J. Stone, and D. Dye: Quaternary alloying effects and the prospects for a new generation of Co-base superalloys. In *Superalloys 2012*, E.S. Huron, R.C. Reed, M.C. Hardy, M.J. Mills, R.E. Montero, P.D. Portella, and J. Telesman, eds. (The Minerals, Metals & Materials Society, Warrendale, PA, 2012); p. 705.
26. M. Feller-Kniepmeier and T. Link: Dislocation structures in $\gamma$–$\gamma'$ interfaces of the single-crystal superalloy SRR 99 after annealing and high temperature creep. *Mater. Sci. Eng., A* **113**, 191 (1989).
27. F. Pyczak, B. Devrient, and H. Mughrabi: The effects of different alloying elements on the thermal expansion coefficients, lattice constants and misfit of nickei-based superalloys investigated by X-ray diffraction. In *Superalloys 2004*, K.A. Green, T.M. Pollock, H. Harada, T.E. Howson, R.C. Reed, J.J. Schirra, and S. Walston, eds. (The Minerals, Metals & Materials Society, Warrendale, PA, 2004); p. 827.
28. K. Tanaka, T. Ohashi, K. Kishida, and H. Inui: Single-crystal elastic constants of $Co_3$(Al,W) with the $L1_2$ structure. *Appl. Phys. Lett.* **91**, 181907 (2007).


https://doi.org/10.1557/jmr.2017.362 Published online by Cambridge University Press

29. N.L. Okamoto, T. Oohashi, H. Adachi, K. Kishida, H. Inui, and P. Veyssière: Plastic deformation of polycrystals of $Co_3(Al,W)$ with the $L1_2$ structure. *Philos. Mag.* **91**, 3667 (2011).
30. S. Kraft, I. Altenberger, and H. Mughrabi: Directional $\gamma$–$\gamma'$ coarsening in a monocrystalline nickel-base superalloy during low-cycle thermomechanical fatigue. *Scr. Metall. Mater.* **32**, 411 (1995).
31. M. Fährmann, E. Fährmann, O. Paris, P. Fratzl, and T.M. Pollock: An experimental study of the role of plasticity in the rafting kinetics of a single crystal Ni-base superalloy. In *Superalloys 1996*, R.D. Kissinger, D.J. Deye, D.L. Anton, A.D. Cetel, M.V. Nathal and D.A. Woodford, eds. (The Minerals, Metals & Materials Society, Warrendale, PA, 1996); p. 191.
32. A. Pineau: Influence of uniaxial stress on the morphology of coherent precipitates during coarsening–elastic considerations. *Acta Metall.* **24**, 559 (1976).
33. S. Kobayashi, Y. Tsukamoto, T. Takasugi, H. Chinen, T. Omori, K. Ishida, and S. Zaefferer: Determination of phase equilibria in the Co-rich Co–Al–W ternary system with a diffusion-couple technique. *Intermetallics* **17**, 1085 (2009).
34. J.E. Saal and C. Wolverton: Thermodynamic stability of Co–Al–W $L1_2$ $\gamma'$. *Acta Mater.* **61**, 2330 (2013).
35. E.A. Lass, M.E. Williams, C.E. Campbell, K-W. Moon, and U.R. Kattner: $\gamma'$ phase stability and phase equilibrium in ternary Co–Al–W at 900 °C. *J. Phase Equilib. Diffus.* **35**, 711 (2014).

https://doi.org/10.1557/jmr.2017.362 Published online by Cambridge University Press